PAPER Nr. : 59

AEROMECHANICAL STABILITY ANALYSIS OF A MULTIROTOR VEHICLE WITH APPLICATION TO HYBRID HEAVY LIFT HELICOPTER DYNAMICS

BY

C. VENKATESAN AND P.P. FRIEDMANN

MECHANICAL, AEROSPACE AND NUCLEAR ENGINEERING DEPARTMENT
UNIVERSITY OF CALIFORNIA
LOS ANGELES, CALIFORNIA 90024, U.S.A.

TENTH EUROPEAN ROTORCRAFT FORUM

AUGUST 28 – 31, 1984 – THE HAGUE, THE NETHERLANDS

AEROMECHANICAL STABILITY ANALYSIS OF A MULTIROTOR VEHICLE WITH APPLICATION TO HYBRID HEAVY LIFT HELICOPTER DYNAMICS*

C. Venkatesan† and P.P. Friedmann††
Mechanical, Aerospace and Nuclear Engineering Department
University of California
Los Angeles, California 90024, U.S.A.

ABSTRACT

The Hybrid Heavy Lift Helicopter (HHLH) is a potential candidate vehicle aimed at providing heavy lift capability at low cost. This vehicle consists of a buoyant envelope attached to a supporting structure. Four rotor systems are also attached to the supporting structure. Non-linear equations of motion capable of modeling the dynamics of this multi-rotor/support frame/vehicle system have been developed and used to study the fundamental aeromechanical stability characteristics of this class of vehicles. The mechanism of coupling between the blades, supporting structure and rigid body modes is identified and the effect of buoyancy ratio (buoyant lift/total weight) on the vehicle dynamics is studied. It is shown that dynamics effects have a major role in the design of such vehicles. The analytical model developed is also useful for studying the aeromechanical stability of single rotor and tandem rotor coupled rotor/fuselage systems.

Nomenclature

a	= Lift curve slope
BR	= Buoyancy ratio (Buoyant lift/total weight of the vehicle)
$[C]$	= Damping matrix
C_T	= Thrust coefficient of the rotor
f	= Rotating natural frequency
F_x, F_y, F_z	= Forces along x,y,z directions of the body axes
h_1	= Distance between origin O_s and underslung load, Fig. 2
h_2	= Distance between centerline and rotor hub, Fig. 2
h_3	= Distance between centerline and center of volume of the envelope, Fig. 2

* This work was supported by NASA Ames Research Center under Grant NAG 2-116
† Assistant Research Engineer
†† Professor of Engineering and Applied Sciences

h_4 = Distance between centerline and C.G. of the envelope, Fig. 2

h_5 = Distance between the origin O_s and C.G. of the structure, Fig. 2

I_{xx}, I_{yy} = Rotary inertia of the vehicle in roll and pitch, respectively

$[K]$ = Stiffness matrix

K_{SBXY}, K_{SBXZ} = Supporting structure bending stiffness in x-y (Horizontal) plane and in x-z (Vertical) plane respectively (in fundamental mode)

K_{ST} = Supporting structure torsional stiffness (in fundamental mode)

$K_\beta, K_\zeta, K_{\phi B}$ = Root spring constant of the blade in flap, lag and torsion respectively

$K_{\phi C}$ = Control system stiffness

K_ϕ = Equivalent spring stiffenss in torsion of the blade

ℓ_{F1}, ℓ_{F2} = Distance between origin O_S and the center of gravity of the fuselages, F_1 and F_2 respectively, Fig. 2

$[M]$ = Mass matrix

M_x, M_y, M_z = Moments about x,y,z axes acting on the vehicle

M_β, M_ζ, M_ϕ = Blade root moments in flap, lag and torsion respectively

N = Number of blades in a rotor (N>2)

P_z^s = Static buoyancy on the envelope

$\{q\}$ = Generalized coordinate vector

R_x, R_y, R_z = Rigid body perturbational motion in x,y,z directions respectively

s_k = k^{th} eigenvalue $(\sigma_k \pm j\omega_k)$; $j=\sqrt{-1}$

T_1, T_2 = Thrust developed by rotor systems R_1 and R_2, respectively

W = Total weight of the vehicle

W_{EN} = Weight of the envelope

W_{F1}, W_{F2} = Weight of the fuselages F_1 and F_2

W_S = Weight of the supporting structure

$W_{S'}$ = Weight of passenger compartment

W_{UN} = Underslung weight

$\{y_1\},\{y_2\}$ = State vector

β_k,ζ_k,ϕ_k = Flap, lead-lag and torsion angles of the k^{th} blade

$\beta^i_{k0},\zeta^i_{k0},\phi^i_{k0}$ = Equilibrium angles in flap, lag and torsion of the k^{th} blade in the i^{th} rotor system i = 1,2

β_0,ζ_0,ϕ_0 = Equilibrium angles in flap, lag and torsion, respectively

$\Delta\beta_k,\Delta\zeta_k,\Delta\phi_k$ = Perturbational quantities in flap, lag and torsion, respectively

β_M,ζ_M,ϕ_M = Generalized coordinates for collective flap, lag and torsion modes

$\beta_{-M},\zeta_{-M},\phi_{-M}$ = Generalized coordinates for alternating flap, lag and torsion modes

$\beta_{1C},\zeta_{1C},\phi_{1C}$ = Generalized coordinates for 1-cosine flap, lag and torsion modes

$\beta_{1S},\zeta_{1S},\phi_{1S}$ = Generalized coordinates for 1-sine flap, lag and torsion modes

β_p,ζ_p,ϕ_p = Progressing (or high frequency) flap, lag and torsion modes

β_R,ζ_R,ϕ_R = Regressing (or low frequency) flap, lag and torsion modes

ϵ = Basic order of magnitude for blade slopes employed in ordering scheme

λ = Inflow ratio

ω_k = Modal frequency in k^{th} mode (imaginary part of s_k)

$\bar{\omega}_{SBXY}$ = Nondimensional uncoupled fundamental bending frequency of the supporting structure in x-y plane

$\bar{\omega}_{SBXZ}$ = Nondimensional uncoupled fundamental bending frequency of the supporting structure in x-z plane

$\bar{\omega}_{ST}$ = Nondimensional uncoupled fundamental torsion frequency of the supporting structure

Ω = Rotor speed of rotation, R.P.M.

σ_k = k^{th} modal damping (real part of s_k)

σ = Solidity ratio

θ_0, θ = Collective pitch of the blade

θ_0^i = Collective pitch setting for the i^{th} rotor

$\theta_x, \theta_y, \theta_z$ = Perturbational rotation in roll, pitch and yaw respectively

ξ_1, ξ_2 = Generalized coordinate for the fundamental mode bending of the supporting structure in x-y plane and x-z plane respectively

ξ_3 = Generalized coordinate for the fundamental torsion mode of the supporting structure

$(\bar{\ })$ = Nondimensional quantity

1. Introduction

Hybrid Heavy Lift Helicopter (HHLH) or Hybrid Heavy Lift Airship (HHLH) is a candidate vehicle for providing heavy lift capability. Potential applications of this vehicle are for logging, construction, coast guard surveillance and military heavy lift. These vehicles combine buoyant envelope lift with lift and control forces generated by a multi-rotor system. A rough sketch of a typical HHLH vehicle is shown in Fig. 1. Clearly such a vehicle is quite different from the conventional rotorcraft. It is well known that aeroelastic and structural dynamic considerations are of primary importance in the successful design of rotary-wing vehicles. The aeroelastic and structural dynamic behavior of HHLH type vehicles has not been considered in the technical literature to date, therefore it is reasonable to consider these topics so that potential aeroelastic instability modes and structural dynamic aspects of such vehicles can be simulated and identified in the design process. Recent studies on HHLH type vehicles dealt with the overall dynamic stability and control of the vehicle under the assumption that it behaves like a rigid body having six degrees of freedom[1,2]. However, the aeroelastic stability of the rotor and the aeromechanical stability of the coupled rotor/support system as well as the interaction of the buoyant lift with these vehicle dynamic characteristics have not been considered in the literature before.

The main objectives of this paper are to develop a fundamental understanding of the aeroelastic and aeromechanical problems which can be encountered in a HHLH type vehicle due to their unique features such as: buoyancy, multiple rotor systems, flexible supporting structure and underslung load.

This study is based on a simplified model of a HHLH type vehicle, in which the salient features are retained. These simplifying assumptions consist of using two rotor systems instead of four, and a beam type structure representing the flexible supporting structure (Fig. 1), which in reality consists of a three dimensional frame (or truss). The essential features of this configuration, illustrated in Fig. 2, are described below:

(a) two rotor systems, providing lift, each having arbitrary number of blades N(N>2) are attached rigidly to the ends of a flexible supporting structure;

(b) the flexible supporting structure is capable of bending in two orthogonal planes (horizontal and vertical) and it can also twist about its longitudinal axis;

(c) an envelope providing buoyant lift, acting at its center of buoyancy, is attached at the center of the supporting structure;

(d) two masses are attached at the two ends of the flexible structure, these two masses represent helicopter fuselages;

(e) a weight W_{UN} simulating an underslung load is attached to the structure.

The dynamic equations of motion for this model were derived in Ref. 3. The equations of motion are nonlinear coupled differential equations and they represent the dynamics of the coupled rotor/support frame/vehicle system in forward flight. The equations of motion can be divided into three groups, each group represnting an appropriate subsystem of equations. These are:

(1) rotor blade equations of motion in flap, lead-lag and torsion, respectively;

(2) rigid body equations of motion of the complete vehicle;

(3) equations of motion of the flexible supporting structure.

These coupled equations of motion have considerable versatility and can be used to study different classes of rotary-wing dynamic problems which are listed below in an ascending order of complexity:

(a) isolated rotor blade aeroelastic stability;

(b) coupled single rotor/supporting structure dynamics, which is representative of coupled rotor/body aeromechanical stability;

(c) stability of tandem rotor and side by side rotor helicopters;

(d) dynamics of HHLH type vehicles, in hover and forward flight.

The results presented in this paper deal primarily with the aeroelastic and aeromechanical stability analysis of an HHLH type of vehicle, shown in Fig. 2. The total number of degrees of freedom used in modeling this system which consists of two four bladed rotors and a flexible

supporting structure is 31. Thus the stability analysis yields a total of 62 eigenvalues corresponding to these 31 degrees of freedom. Based on a careful parametric study, the various blade and vehicle modes have been identified. The physical interpretation of the various eigenvalues is determined from a systematic study of the eigenvalue changes caused by variations of the vehicle system parameters. Furthermore the coupling between various blade and vehicle modes is identified. Finally vehicle stability is analyzed at different buoyancy ratios (BR = Buoyancy of the envelope/total weight of the vehicle) so as to determine the influence of buoyancy on the aeromechanical stability of the vehicle.

2. Equations of Motion

Recent research on rotary-wing aeroelasticity[4] has indicated that geometrically nonlinear effects, due to moderate blade deflections, are important for this class of problems. Thus a proper treatment of rotary-wing aeroelastic problems requires the development of a consistent mathematical model, which includes the geometrically nonlinear effects associated with finite blade slopes in the aerodynamic, inertia and structural operators. Retention of the nonlinear terms is based on an ordering scheme[3,4]. All the important parameters of the problem are assigned orders of magnitude in terms of a nondimensional quantity ε, which represents the typical blade slope ($0.1<\varepsilon<0.15$). The ordering scheme consists of neglecting terms of the order $O(\varepsilon^2)$ when compared to unity, i.e., $1 + \varepsilon^2 \simeq 1$.

The most important assumptions used in formulating the equations of motion are: (1) each rotor consists of three blades or more, (2) the rotors are lightly loaded, (3) the rotor is in uniform inflow, (4) the rotor blade is modelled as a rigid blade model with orthogonal root springs (Fig. 3). This blade model is useful for simulating configurations which are either hingeless or articulated, (5) there is no aerodynamic interference between the rotor and the buoyant envelop, (6) the aerodynamic model used for the rotor is a quasi-steady blade element theory based on Greenberg's[5] derivation of unsteady aerodynamic loads on an oscillating airfoil in a pulsating flow, and (7) the elastic supporting structure is modelled as a free-free beam for which the bending and torsional structural dynamics are modelled by the corresponding free vibration modes.

The various degrees of freedom considered for the model vehicle are: flap (β_k), lead-lag (ζ_k), torsion (ϕ_k) for each blade, rigid body translation (R_x, R_y, R_z) and rigid body rotation ($\theta_x, \theta_y, \theta_z$) of the vehicle as a whole and the generalized coordinates representing the uncoupled normal modes of vibration of the supporting structure (ξ_1, ξ_2, ξ_3). The equations of motion for the blade are obtained by enforcing moment equilibrium, of the various forces on the blade, at the root. The blade equations are written in a hub fixed rotating reference frame and these equations have periodic coefficients. The rigid body equations of motion are obtained by imposing the force and moment equilibrium of the vehicle. The equations of motion for the elastic modes of the supporting structure are obtained using a normal mode approximation. The complete details and the derivation can be found in Ref. 3. An overview of the coupling process between the blade motion and the body motion is presented in Fig. 4, which is a schematic diagram describing the basic operations involved in the derivation of equations of motion for the coupled multi-rotor/vehicle system. It can be seen from Fig. 4 that the

rigid body motions of the vehicle and the elastic deformations of the supporting structure are affected by the rotor loads. In turn, these rotor loads are related to the rigid body motions and the elastic deformation through the hub motions.

The final set of equations of motion are nonlinear ordinary differential equations with periodic coefficients. These equations have to be solved so as to determine the aeroelastic and aeromechanical stability characteristics of the vehicle.

3. Method of Solution

The method of solution for the coupled rotors/vehicle problem follows essentially the procedure outlined in Refs. 4 and 6. A brief description of the procedure aimed at determining the aeroelastic and aeromechanical stability characteristics of the vehicle is provided below.

1. Calculation of the equilibrium state of an individual blade and the trim setting of the blade collective pitch angle.

2. Linearization of the nonlinear ordinary differential equations about the equilibrium position (linearized equations will have periodic coefficients).

3. Transformation of the linearized equations with periodic coefficients to linearized equations with constant coefficients, using multi-blade coordinate transformation[7,8].

4. Evaluation of the eigenvalues of the linearized system with constant coefficients to obtain information on the stability of the vehicle.

The four steps described above represent essentially two separate stages of the analysis. The first stage consists of a trim analysis by which the equilibrium position of the blade is determined. Subsequently in the second stage a stability analysis of the linearized perturbational equations about the equilibrium state is carried out.

3.1 Trim or Equilibrium State Solution

In the trim analysis, the force and moment equilibrium of the complete vehicle together with the moment equilibrium of the individual blade about its root in flap, lead-lag and torsion are enforced. It is important to recognize that only the generalized coordinates representing the blade degrees of freedom will have a steady state value representing the equilibrium position. The generalized coordinates associated with the rigid body motions of the vehicles are essentially perturbational quantities and hence their equilibrium, or trim values are identically zero. In deriving the equations of motion for the flexible supporting structure, it was assumed that the vibrations of the structure occur about a deflected equilibrium position. The determination of the equilibrium of the supporting structure is unimportant, for the case considered in this study because: (a) The equilibrium deflection (or position) of the supporting structure does not affect the equilibrium values of the blade degrees of freedom, since the blade equations contain only the terms with the time derivatives of the degrees of freedom representing the elastic modes of the supporting structure. The physical reason for this

mathematical dependence is due to the fact that the blade inertia and aerodynamic loads depend on the hub motion and not on the hub equilibrium position (the hub motion is related to the fuselage motion and the vibration of the supporting structure), and (b) the final linearized differential equations used for the stability analysis do not contain any term dependent on the static equilibrium deflection of the supporting structure. Hence, the generalized coordinates for the vibration modes of the supporting structure can be also treated as perturbational quantities. However, it should be noted that the evaluation of the static equilibrium deflection of the supporting structure could be important in the proper design of the supporting structure.

The k^{th} blade degrees of freedom can be written as

$$\begin{aligned} \beta_k &= \beta_{k0} + \Delta\beta_k(\psi) \\ \zeta_k &= \zeta_{k0} + \Delta\zeta_k(\psi) \\ \phi_k &= \phi_{k0} + \Delta\phi_k(\psi) \end{aligned} \tag{1}$$

where β_{k0}, ζ_{k0}, ϕ_{k0} are the steady state values and $\Delta\beta_k$, $\Delta\zeta_k$, $\Delta\phi_k$ are the perturbational quantities.

Linearization of the equations is accomplished by substituting these expressions into the nonlinear coupled differential equations and neglecting terms containing the products or squares of the perturbational quantities. The remaining terms are then separated into two groups: one group of terms contains only the steady state quantities and constants (i.e., time independent quantities). These represent the trim or equilibrium equations. For the case of hover, these are nonlinear algebraic equations which represent the force and moment equilibrium equations determining the steady state. The second group contains the time dependent perturbational quantities and represents the equations of motion about the equilibrium position. The linearized dynamic equations of equilibrium are used for the stability analysis.

The steady state equilibrium equations can be written symbolically as:

for the complete vehicle

$$F_x = F_y = F_z = 0 \tag{2}$$

$$M_x = M_y = M_z = 0 \tag{3}$$

and for the individual blade

$$M_\beta = M_\zeta = M_\phi = 0 \tag{4}$$

In the above equations F_x, F_y, and M_x are identically zero. The remaining equations for the vehicle can be written as

$$F_z = T_1 + T_2 + P_z^s - W = 0 \tag{5}$$

$$M_y = 0 \tag{6}$$

$$M_z = 0 \tag{7}$$

where T_1 and T_2 are the thrust developed by the two rotor systems R_1 and R_2 respectively, P_z^s in the static buoyancy due to the envelope and W is the weight of the complete vehicle. The quantities T_1 and T_2 are functions of the steady state flap, lead-lag and torsion angles, collective pitch angles and the operating conditions of the rotor. Equation (7) for M_z represents the torques developed by the two rotor systems. These torques can either be balanced by having a tail rotor for each main rotor or by having two counter-rotating main rotors. In the present study, it is assumed that the torques are balanced by tail rotors. Equation (6) for M_y consists of the pitching moments developed by the thrust due to the rotors and the gravity loads acting on the various components.

The steady state moment equilibrium equations for the individual blade will have the following symbolic form

$$M_\beta = f_1^i \left(\beta_{k0}^i, \xi_{k0}^i, \phi_{k0}^i, \theta_0^i\right) = 0 \tag{8}$$

$$M_\zeta = f_2^i \left(\beta_{k0}^i, \zeta_{k0}^i, \phi_{k0}^i, \theta_0^i\right) = 0 \tag{9}$$

$$M_\phi = f_3^i \left(\beta_{k0}^i, \zeta_{k0}^i, \phi_{k0}^i, \theta_0^i\right) = 0 \tag{10}$$

where i = 1,2 refer to the two rotor systems R_1 and R_2 respectively and k refers to the k^{th} blade in the i^{th} rotor system. For the case of hover, all the blades in one particular rotor system will have the same steady state values (i.e., equilibrium quantities). Thus the subscript 'k' can be deleted.

Equations (5), (6), (8)-(10) are nonlinear algebraic equations. These are a total of eight equations and 8 variables ($\beta_0^i, \zeta_0^i, \phi_0^i, \theta_0^i$; l=1,2). These eight equations are solved iteratively using the Newton-Raphson method, to obtain the steady state values. Failure to converge during iteration is attributed to divergence or static instability of the blade.

In deriving the equations of motion, the inflow ratio λ is assumed to be constant over the rotor disc. The typical value chosen for the inflow ratio is its value at 75% of the blade span. It is given as

$$\lambda = \frac{\sigma a}{16}\left(-1 + \sqrt{1 + \frac{24\theta_0}{\sigma a}}\right) \tag{11}$$

3.2 Description of Stability Analysis

The perturbational equations of motion, linearized about the equilibrium position, can be written in the following form

$$[M]\{\ddot{q}\} + [C]\{\dot{q}\} + [K]\{q\} = 0 \tag{12}$$

where {q} contains all the degrees of freedom representing the blade motion, the rigid body motions of the vehicle and the flexible modes of the supporting structure.

The matrices [M], [C] and [K] can be identified as representing mass, damping and stiffness matrices respectively and the elements of these matrices are functions of the equilibrium values.

The stability of the vehicle about the trim condition is obtained by solving the eigenvalue problem represented by Eq. (12). For convenience Eq. (12) is rewritten in state variable form

$$\{\dot{y}\} = [F]\{y\} \tag{13}$$

where $\{y\}^T = \{y_1\}^T, \{y_2\}^T$

and $\{y_1\} = \{\dot{q}\}; \{y_2\} = \{q\}$

and

$$[F] = \left[\begin{array}{c|c} -[M]^{-1}[C] & -[M]^{-1}[K] \\ \hline [I] & [0] \end{array}\right]$$

Assuming a solution for Eq. (13) in the form of $\{y\} = \{\bar{y}\}e^{s\psi}$, yields the standard eigenvalue problem

$$[F]\{y\} = s\{y\} \tag{14}$$

The eigenvalues of Eq. (14) can be either real or complex conjugate pairs

$$s_k = \sigma_k \pm i\omega_k$$

The complex part of the k^{th} eigenvalue (ω_k) refers to the modal frequency and the real part (σ_k) refers to the modal damping. The mode is stable when $\sigma_k<0$ and the stability boundary is represented by $\sigma_k = 0$.

This relatively simple procedure can become complicated depending on the form of the matrices [M], [C] and [K]. In the aeroelastic stability analysis of a isolated rotor in hover, these matrices contain constant elements. Thus the solution of this eigenvalue problem is straight-forward. However when dealing with the stability analysis of a coupled rotor/vehicle system in hover, as required in the present case, these matrices will have elements which are time dependent. The reason for the appearance of time dependent or periodic coefficients is due to the vehicle perturbational motion and vibration of the supporting structure. These perturbational motions introduce, through the hub motion, periodic terms in inertia and aerodynamic loads of the blade.

For the cases, when the matrices in the linearized perturbational equations are time dependent, the stability analysis can be performed by applying either Floquet theory or by using a multiblade coordinate transformation[7,8]. It is well known that for the coupled rotor/vehicle type of analysis for the case of hover, the multiblade coordinate transformation is successful in eliminating the time dependency of the coefficients, in the equations of motion. During this transformation, the individual blade degrees of freedom will transform into a new set of rotor degrees of freedom. These rotor degrees of freedom are basically representative of the behavior of the rotor as a whole when viewed from a non-rotating reference frame. The various rotor degrees of freedom are known as collective, cyclic and alternating degrees of freedom. For

example, in a four bladed rotor, the flap degree of freedom corresponding to each blade (β_k; k = 1,4) will transform into collective flap (β_M), cyclic flap (β_{1c},β_{1s}) and alternating degree of (β_{-M}) degrees of freedom. Alternating degrees of freedom will appear only when the rotor consists of an even number of blades. In a similar fashion, the lead-lag and torsional degrees of freedom will also transform into corresponding rotor degrees of freedom.

As a result of the application of the multiblade coordinate transformation, the linearized perturbational equations with periodic coefficients will transform into linearized perturbational equations with constant coefficients. Using these equations, with constant coefficients, a stability analysis is performed as described above. The eigenvalues corresponding to the cyclic degrees of freedom of the rotor (β_{1c},β_{1s},ζ_{1c},ζ_{1s},ϕ_{1c},ϕ_{1s}) are referred in this paper as high frequency (or progressing) and low frequency (or progressing or regressing) mode. The designation of high frequency or low frequency mode is based on the rotating natural frequency of the rotor. Suppose, the rotating natural frequency, say in lead-lag, is f/rev, then the two frequencies corresponding to the cyclic modes (ζ_{1c},ζ_{1s}) will be usually (f+1)/rev and (f-1)/rev. The mode with the frequency (f+1)/rev. is called a high frequency lag mode and that corresponding to (f-1)/rev. is called a low frequency lag mode. The mode with the frequency f/rev. is known as the collective lag mode. Since the HHLH model vehicle (Fig. 2) consists of two rotor systems coupled by a supporting structure, the stability analysis will provide a pair of eigenvalues for each rotor degree of freedom. Hence for the purpose of identification, in the presentation of the results the rotor modes will be referred to as mode 1 and mode 2, such as collective flap mode 1, collective flap mode 2 and high frequency flap mode 1 and high frequency flap mode 2, etc.

4. Results and Discussion

The validity of the equations of motion for the coupled rotor/vehicle system was first verified by using them to solve the aeromechanical stability problem of a single rotor helicopter in ground resonance and comparing the analytical results, obtained using our equations, with experimental data presented in Ref. 9. We found that our analytical results are in good agreement with the experimental results indicating that the equations of motion for the coupled rotor/vehicle system are valid. Sample results taken from Ref. 10, are included in this paper to illustrate the degree of correlation. Figure 5 presents the variation of rotor and body frequencies with rotor speed Ω. Fig. 6 presents the variation of damping in the lead-lag regressing mode with Ω. Figure 7 shows the variation of the regressing lag mode damping as a function of the collective pitch setting of the blade. It is evident from these figures that our analytical prediction are in good agreement with the experimental results.

The stability of the model vehicle (Fig. 2) representing an HHLH is analyzed for the case of hovering flight. The various degrees of freedom considered for this problem are flap, lead-lag, torsion (for each blade), rigid body translation (R_x,R_y), rigid body rotation (θ_x,θ_y) and three normal modes of vibration of the supporting structure. The three normal modes represent the fundamental symmetric bending mode (ξ_1) in the horizontal (x-y) plane, the fundamental symmetric bending mode (ξ_2) in the vertical (x-z) plane and the fundamental antisymmetric

torsion (ξ_3) about the longitudinal axis. For a four bladed rotor, there are in total 31 degrees of freedom, namely 12 rotor degrees of freedom for each rotor,plus four rigid body degrees of freedom plus three elastic vibration modes of the supporting structure. Hence a stability analysis for this system will yield 62 eigenvalues corresponding to these 31 degrees of freedom. The primary aim is to identify the 62 eigenvalues and relate them to the various modes of the rotor/vehicle assembly. This relatively complicated identification process is based on physical insight gained by performing some preliminary calculations augumented by additional considerations described below:

1. Comparison of the imaginary part of the eigenvalue (ω) with the uncoupled frequencies of the various modes, and

2. Use of an extensive study in which the primary parameters allowed to vary are the bending and torsional stiffness of the supporting structure (K_{SBXY},K_{SBXZ},K_{ST}) combined with the rotary inertia of the vehicle in pitch (I_{yy}) and roll (I_{xx}).

Based on the results obtained in the parametric study, the various eigenvalues and the coupling among different modes are identified. It should be noted that for the cases studied, the trim (or equilibrium) quantities are the same because the trim values are independent of the quantities varied in the parametric study. A complete description of this study can be found in Ref. 6.

For the example problem analyzed, the rotors are articulated and they are identical. The data used for this study is presented in Appendix A. The result presented below are obtained for the model vehicle without the sling load.

The results of the trim (or equilibrium) analysis are presented in Appendix B. Since the two rotors have identical geometrical properties and identical operating conditions and furthermore the model vehicle possesses a symmetry about y-z plane, the equilibrium angles of the blade are the same for both rotor systems. For the buoyancy ratio of BR = 0.792, the thrust coefficient in the rotors is $C_T = 0.00158$. The equilibrium blade angles are in flap $\beta_0 = 2.302$ deg., in lead-lag $\zeta_0 = -3.963$ deg. and in torsion $\phi_0 = -0.115$ deg. The collective pitch angle is $\theta_0 = 4.206$ deg.

The results of the stability analyses are presented in Figs. 8-12. Figure 8 illustrates the variation of the eigenvalues of blade lead-lag modes and the supporting structure bending modes due to an increase in the bending stiffness (K_{SBXY}) of the supporting structure in x-y (horizontal) plane. The bending stiffness K_{SBXY} was increased in increments from 5.09×10^7 N/m to 1.74×10^8 N/m, such that the corresponding uncoupled nondimensional bending frequency in x-y plane ($\bar{\omega}_{SBYX}$) assumed the values $\bar{\omega}_{SBXY} = 1.2, 1.499, 1.754, 2.192$, where the frequencies are nondimensionalized with respect to the rotor speed of rotation Ω, where $\Omega = 217.79$R.P.M.. The arrows in the figure indicate the direction along which the eigenvalues of the modes change due to an increase in K_{SBXY}. The eigenvalues of the other modes, which are not shown in the figure, remain unaffected by the variation in K_{SBXY}. It can be seen from Fig. 8 that the bending mode, in x-y plane, of the supporting structure is strongly coupled with the high frequency lag mode 2. The high frequency lag mode 2, which was initially unstable, becomes more stable as K_{SBXY} is increased. The damping in the bending mode in x-y plane decreases asymptotically with an

increase in frequency and this mode is always stable. The low frequency lead-lag mode 2 shows a slight decrease in damping as K_{SBXY} is increased. The eigenvalues corresponding to the bending mode in x-z plane and the high frequency lag mode 1 are not affected by the changes in K_{SBXY}. However, since these two modes have nearly equal frequencies it can be seen that the high frequency lag mode 1 is unstable.

Figure 9 presents the variation of eigenvalues of the blade lead-lag modes and the supporting structure bending modes as a result of an increase in the bending stiffness (K_{SBXZ}) of the supporting structure in x-z (vertical) plane. The bending stiffness K_{SBXZ} was increased in increments from 7.96×10^6 N/m to 1.74×10^8 N/m and the corresponding nondimensional uncoupled bending frequency in x-z plane ($\bar{\omega}_{SBXZ}$) assumed the values $\bar{\omega}_{SBXZ} = 1.499, 1.754, 2.192$. It can be seen from Fig. 9 that the bending mode in x-z plane is strongly coupled with high frequency lag mode 1. The high frequency lag mode 1, which was initially unstable, becomes a stable mode as K_{SBXZ} is increased from 7.96×10^7 N/m ($\bar{\omega}_{SBXZ} = 1.499$) to 1.09×10^8 N/m ($\bar{\omega}_{SBXZ} = 1.754$). Further increase in K_{SBXZ} to 1.74×10^8 N/m does not affect the eigenvalue corresponding to the high frequency lag mode 1, indicating that these two modes are decoupled. Damping in the bending mode in x-z plane decreases drastically at the beginning and once the bending mode and the high frequency lag mode 1 are decoupled, the decrease in damping of the bending mode in x-z plane is very small. Damping in the torsion mode of the supporting structure and low frequency lag mode 1 are slightly affected as K_{SBXZ} is increased. Since the torsion mode and the low frequency lag mode 1 have frequencies which are close to each other, the figure clearly indicates that the lag mode 1 is unstable. The eigenvalues corresponding to the rest of the modes are unaffected by this parameter variation.

Figure 10 shows the eigenvalue variation in the rotor lead-lag modes and the torsion mode of the supporting structure as a result of an increase in the torsional stiffness (K_{ST}) of the supporting structure. The torsional stiffness, K_{ST}, was increased in increments from $K_{ST} = 1.59 \times 10^6$ N.m to 3.99×10^7 N.m and the corresponding uncoupled nondimensional torsional frequency ($\bar{\omega}_{ST}$) of the supporting structure are $\bar{\omega}_{ST} = 0.4, 0.55, 0.846, 1.096, 1.2, 1.3, 1.4, 1.5, 1.754, 2.0$. It is evident from the figure that the low frequency lag mode 2 and high frequency lag mode 2 remain unaffected during the variations in K_{ST} and these modes are stable. In Fig. 10, the different curves are divided into three segments represented by points A, B, C, and D. The curves between points A to B refer to the range of $K_{ST} = 3.01 \times 10^6$ N.m to 7.20×10^6 N.m ($\bar{\omega}_{ST} = 0.55$ to 0.846); the curves between points B to C refer to the range $K_{ST} = 7.20 \times 10^6$ N.m to 1.685×10^7 N.m ($\bar{\omega}_{ST} = 0.846$ to 1.3); and the curves between points C to D refer to the range $K_{ST} = 1.685 \times 10^7$ N.m to 3.1×10^7 N.m ($\bar{\omega}_{ST} = 1.3$ to 1.754).

It is evident from Fig. 10 that in the range A to B, as the torsional stiffness K_{ST} is increased, the torsion mode of the supporting structure becomes increasingly stable and its frequency is increasing; the low frequency lag mode 1 becomes increasingly unstable and its frequency increases slightly. This clearly indicates that the torsion mode is strongly coupled with the low frequency lag mode 1. The high frequency lag mode 1 experiences a slight increase in frequency but its damping remains almost unchanged. In this range, A to B, the eigenvalues of these three modes have been distinctly identified based on their uncoupled nondimensional frequencies. In the range B to C, as the torsional

stiffness K_{ST} is increased, the damping in the low frequency lag mode 1 decreases and its frequency tends to increase towards 1.0. At the same time, the damping in torsional mode of the supporting structure decreases drastically and a slight change in the frequency is observed (i.e., the frequency initially increases and then decreases). The high frequency lag mode 1 shows an increase in frequency with no appreciable change in damping. In this range B to C, the eigenvalues of these three modes do not exhibit a direct one to one correspondence to the uncoupled nondimensional frequencies, implying that all these modes are coupled. Hence in this range, B to C, the reference to the various modes, as torsion mode, low frequency lag mode 1 and high frequency lag mode 1, is only for the convenience of explaining the variation of the eigenvalues. When the torsional stiffenss K_{ST} was increased still further, i.e., the range C to D, the eigenvalues start exhibiting a correspondence to non-dimensional uncoupled frequencies indicating that these three modes are slowly decoupled. In this range, C to D, the torsional mode of the supporting structure has low damping and it tends to decrease asympotically while the frequency increases from 1.5 to 1.75. The high frequency lag mode 1 shows an increase in the frequency and the mode becomes stable at the point D. The damping in the low frequency lag mode 1 decreases while the frequency undergoes a slight reduction. Beyond the point D i.e., for $K_{ST} \geq 3.1 \times 10^7$ N.m the eigenvalues of low frequency lag mode 1 and high frequency lag mode 1 show negligible change and the damping in torsion mode remains the same but its frequency increases. Beyond point D all the three modes are stable.

Another interesting observation which can be made from Fig. 10 is due to the increase in torsional stiffness K_{ST}. When K_{ST} is increased from 1.685×10^7 N.m to 3.99×10^7 N.m (curve in the range C to D and beyond), the eigenvalues corresponding to the high frequency lag mode 1 tend to approach the eigenvalue corresponding to the high frequency lag mode 2 (which remains unaffected during the variation in K_{ST}) and similarly the low frequency lag mode 1 approaches the low frequency lag mode 2. This behavior seems to indicate that, as the torsional stiffness of the supporting structure is increased, the coupling between the two rotors due to the torsional deformation of the supporting structure is eliminated. As a result the eigenvalues corresponding to the high frequency lag modes 1 and 2 and low frequency lag modes 1 and 2 approach each other. It should be noted that elimination of the coupling of the two rotors, due to the torsional deformation of the supporting structure, does not imply that the two rotors are totally decoupled. The rotors are still coupled through the bending deformation of the supporting structure and rigid body pitch motion of the vehilce. The presence of this coupling causes the eigenvalues of the low frequency and high frequency lag modes to approach each other rather than coalescing.

It is also evident from Fig. 10 that the high frequency lag mode 1, low frequency lag mode 1 and torsion mode of the supporting structure undergo a reversal in their characteristics as K_{ST} is increased from 1.59×10^6 N.m to 3.99×10^7 N.m. Thus, the mode which was initially a torsion mode becomes a low frequency lag mode 1; the low frequency lag mode 1 becomes a high frequency lag mode 1 and the high frequency lag mode 1 becomes a torsion mode. For low and high values of the torsional stiffness (i.e., $K_{ST} \leq 1.59 \times 10^6$ N.m ($\bar{\omega}_{ST} \leq 0.4$) and $K_{ST} \geq 3.10 \times 10^7$ N.m ($\bar{\omega}_{ST} \geq 1.754$)) the torsional mode of the supporting structure, the low frequency lag mode 1 and high frequency lag mode 1 are all stable. For intermediate values of the torsional stiffness of the supporting structure, one of the lag modes is unstable.

The variation of the eigenvalues of the collective flap modes and body pitch mode due to increase in body inertia in pitch is presented in Fig. 11. It is evident from the figure that the pitch mode is a pure damped mode. An increase in pitch inertia causes the eigenvalues, corresponding to the pitch mode, to approach each other. The eigenvalues of the collective flap mode 2 tend to approach the eigenvalue of the collective flap mode 1. The pure damped nature of the pitch mode is associated with the presence of two rotors. During pitch motion, the net inflow in the two rotor system changes. If in one rotor system the net inflow increases, then in the other one the inflow decreases and vice versa. These changes in inflow result in changes in the thrust in the two rotor systems. The rotor system which moves up, during pitch motion, experiences a reduction in thrust due to the increased inflow and the rotor system which moves down produces more thrust due to the decreased flow. These changes in the thrust tend to restore the vehicle to its equilibrium position. Since this restoring force is proportional to the pitch rate, this mechanism produces a damping in pitch. In the present case, the pitch motion is overdamped. Hence an increase in inertia causes the eigenvalues, corresponding to the pitch mode, to approach each other, as shown in Fig. 11.

Figure 12 illustrates the variation of eigenvalues corresponding to the low frequency lag mode 2 and body roll mode as a result of an increase in inertia in roll. An increase in roll inertia tends to decrease in the damping in roll, furthermore its frequency is also reduced. The low frequency lag mode 2 tends to become more stable. The roll mode, for the model vehicle, is a damped oscillatory mode. This is different from the pure damped mode[7] normally observed in a conventional tandem rotor helicopter. The reason for this oscillatory nature of the roll mode is due to the presence of the buoyancy of the envelope.

For all the cases analyzed, it was found that the flap and torsional modes of the rotor are always stable. The eigenvalues corresponding to the cyclic flap modes and all the torsion modes are not affected by the variation in the quantities used in this parametris study. The alternating modes of the rotor were also found stable.

The degree of coupling, as well as the relative strength of the coupling between the various blade modes and the body modes is presented in a qualitative manner in Table I. It is evident from this table that the supporting structure elastic modes are strongly coupled with the low frequency and high frequency lead-lag modes.

It is interesting to compare, qualitatively, the rigid body modes of an HHLH type vehicle with those of a conventional tandem rotor helicopter. In the literature[7] the longitudinal and lateral dynamics of a tandem rotor helicopter, in hover, are described by six eigenvalues, namely; (a) a pure damped root for pitch; (b) a complex conjugate pair of slightly divergent oscillatory roots for combined pitch and longitudinal translational motion, (c) a pure damped root for roll and (d) a complex pair of divergent oscillatory roots for combined roll and lateral translation. By comparison the results obtained for the HHLH vehicle, shown in Fig. 2, yield the following six eigenvalues corresponding to rigid body modes: (a) two pure damped roots for pitch; (b) a complex pair of damped oscillatory roots for roll and (c) a complex pair of very slightly divergent oscillatory roots for the rigid body translational motions in the longitudinal and lateral directions.

Comparing these two sets of eigenvalues it is evident that for tandem rotor helicopters, the pitch and roll modes are coupled with translational motions which yield divergent oscillatory roots. On the other hand for HHLH type vehicles, the pitch and roll modes are decoupled from the translational motions. This difference in behavior, evident from our parametric study, can be attributed to the following physical effects. For a tandem rotor helicopter the variation of rotor loads, due to perturbational motion in one rigid body mode, influences also the response of the other rigid body modes. For the HHLH type vehicle the buoyant lift of the envelope supports 80% of the total vehicle weight. Thus, variations in rotor loads, due to perturbational motion in a rigid body mode, has negligible effect on the response of the other rigid body modes. When the buoyant lift is set equal to zero the HHLH vehicle reverts to the rigid body dynamic behavior encountered in tandem rotor helicopters. The effects of buoyancy ratio variation on vehicle stability is presented in Table II and Figs. 13 and 14. Table II shows the results from the trim analysis, at various buoyancy ratios. As the buoyancy ratio is decreased, the equilibrium angles of the blade and the thrust coefficient of the rotors increases.

Figure 13 depicts the variation of eigenvalues for the supporting structure elastic modes as a result of a decrease in buoyancy ratio. The direction of arrows in the figure indicate the variation of the eigenvalues as a result of the decrease in buoyance ratio. The frequencies corresponding to these modes are not affected by the variation in buoyancy ratio. However, the damping in bending in x-y plane increases, the damping in bending in x-z plane decreases while the damping in torsion mode increases.

Figure 14 presents the variation of the eigenvalues of pitch and roll modes with buoyance ratio. As the buoyancy ratio is decreased, one of the eigenvalues corresponding to the pitch mode decreases while the other eigenvalue increases. The pitch mode always remains as a pure damped mode. The roll mode which was initially a stable mode becomes unstable for buoyancy ratios BR $\leq$ 0.6.

The results obtained also indicate that as the buoyancy ratio is decreased, the damping in lead-lag modes of the rotors increases while the damping in flap and torsion modes of the rotor decreases. However changes in the buoyancy ratio have only a minor effect on the frequencies of the blade modes. A quantitative indication for the magnitude of the changes in damping in the blade modes produced by changes in the buoyancy ratio is illustrated by the following results: for a 40% reduction in buoyancy ratio, the damping in torsion modes decreases by 12%; the damping in flap modes decreases by 12% and the damping in lag modes increases by 200%.

5. Concluding Remarks

This paper presents the results of an aeromechanical stability analysis of a model vehicle representative of a HHLH configuration in hover. The most important conclusions obtained in this study are presented below.

1) The rotor cyclic lead-lag modes couple strongly with the bending modes and the torsion mode of the supporting structure, as a consequence, the stability of the lead-lag modes is sensitive to changes in stiffness (or the natural frequencies) of the supporting structure in bending and torsion. Therefore the natural frequencies of the supporting

structure must be designed so as to be well separated from the frequencies of the rotor lead-lag modes. This also emphasizes the importance of modelling the supporting structure with an adequate number of elastic modes.

2) The low frequency and high frequency lead-lag modes of the rotor and the torsion mode of the supporting structure undergo a change in their basic characteristics, as the torsional stiffness of the supporting structure is increased from a low value to a high value (i.e., K_{ST} = 1.59 x 10^6 N.m to 3.99 x 10^7 N.m).

3) The lead-lag modes of the rotor are stable only when the torsional stiffness of the supporting structure has low or high values ($K_{ST} \leq$ 1.59 x 10^6 N.m and $K_{ST} \geq$ 3.10 x 10^7 N.m). For intermediate values of K_{ST}, one of the lead-lag modes is unstable.

4) The body pitch mode is a pure damped mode.

5) The body roll mode is a damped oscillatory mode. However, as the buoyancy ratio is decreased, this mode becomes unstable.

6) The stability of the coupled/rotor vehicle dynamics clearly illustrates the fundamental features of the aeroelastic stability of the rotor, coupled rotor/support system aeromechanical stability and the vehicle dynamic stability in longitudinal and lateral planes.

Furthermore, it should be mentioned that the analytical model developed in this study, for the aeromechanical stability study of an HHLH type of vehicle, can be also applied to various other types of vehicles, such as a tandem rotor helicopter configuration and the coupled rotor/body aeromechanical problem of a single rotor helicopter. Finally, it should be noted that the analytical model is capable of representing not only aeroelastic and aeromechanical problems but it is also suitable for investigating rigid body stability and control problems associated with these types of vehicles.

Acknowledgement

The authors would like to express their gratitude to the grant monitor Dr. H. Miura for providing a large part of the data used in these calculations, and also for his constructive comments and suggestions.

References

1. "A Preliminary Design Study of a Hybrid Airship for Flight Research", by Goodyear Aerospace Corporation, NASA CR 166246, July 1981.

2. Tischler, M.B., Ringland, R.F., and Jex, H.R., "Heavy-Lift Airship Dynamics", Journal of Aircraft, Vol. 20, No. 5, May 1983, pp. 425-433.

3. Venkatesan, C. and Friedmann, P.P., "Aeroelastic Effects in Multirotor Vehicles with Application to Hybrid Heavy Lift System, Part I: Formulation of Equations of Motion", NASA Contractor Report, in Press.

4. Friedmann, P.P., "Formulation and Solution of Rotary-Wing Aeroelastic Stability and Response Problems", Vertica, Vol. 7, No. 2, pp. 101-141, 1983.

5. Greenberg, J.M., "Airfoil in Sinusoidal Motion in a Pulsating Flow", NACA TN 1326, 1947.

6. Venkatesan, C. and Friedmann, P.P., "Aeroelastic Effects in Multirotor Vehicles, Part II: Method of Solution and Results Illustrating Coupled Rotor/Body Aeromechanical Stability", NASA CR Report being reviewed for publication.

7. Johnson, W., Helicopter Theory, Princeton University Press, Princeton, New Jersey, 1980.

8. Levin, J., "Formulation of Helicopter Air-Resonance Problem in Hover with Active Controls", M.Sc. Thesis, Mechanics and Structures Department, University of California, Los Angeles, Sept. 1981.

9. Bousman, W.G., "An Experimental Investigation of the Effects of Aeroelastic Couplings on Aeromechanical Stability of a Hingeless Rotor Helicopter", Journal of the American Helicopter Society, Vol. 26, No. 1, Jan. 1981, pp. 46-54.

10. Friedmann, P.P. and Venkatesan, C., "Comparison of Experimental Coupled Helicopter Rotor/Body Stability Results with a Simple Analytical Model", Paper Presented at the Integrated Technology Rotor (ITR) Methodology Workshop, NASA Ames Research Center, Moffett Field, California, June 20-21, 1983, to be published in Journal of Aircraft.

11. Bisplinghoff, R.L., Ashley, H., and Halfman, R.L., Aeroelasticity, Addisonwesley, 1955.

TABLE I: COUPLING BETWEEN BLADE MODES, BODY MODES AND SUPPORTING STRUCTURE MODES

MODES	Lead-lag Modes						Flap Modes					
	High freq.		collective freq.		Low freq.		High freq.		collective freq.		Low freq.	
	1	2	1	2	1	2	1	2	1	2	1	2
Supporting structure symmetric bending in x-y (horizontal) plane		XXX				XX						
Supporting structure symmetric bending in x-z (vertical) plane	XXX		X		XX				X			
Supporting structure torsion(antisymmetric)	XXX				XXX							
Body pitch		X		X		X				X		
Body roll		X				XX						

Legend: XXX = Strongly coupled, XX = Moderately coupled, X = Weakly coupled

TABLE II: EQUILIBRIUM VALUES AT VARIOUS BUOYANCY RATIOS

Buoyancy Ratio BR	θ_0	β_0	ζ_0	ϕ_0	λ	C_T
0.792	4.206°	2.302°	-3.963°	-0.115°	0.03272	.00158
0.7	5.243°	3.209°	-5.074°	-0.161°	0.03820	.00228
0.6	6.259°	4.179°	-6.453°	-0.236°	0.04313	.00304
0.5	7.207°	5.142°	-7.994°	-0.352°	0.04743	.00380

$\bar{\omega}_{ST} = 1.754$, $\bar{\omega}_{SBXY} = \bar{\omega}_{SBXZ} = 2.192$, $I_{yy} = 4.74 \times 10^6$ kg.m^2,

$I_{xx} = 2.0 \times 10^6$ kg.m^2

Appendix A

Blade Data

The HHLH model (Fig. 2) has identical rotors.
Type of rotor: Articulated rotor

Number of blades	N	4
Blade chord	c = 2b	41.654 cm
Hinge offset	e	30.48 cm
Rotor radius	R	8.6868 m
Blade precone	β_p	0
Distance between elastic center and aerodynamic center	X_A	0
Distance between elastic center and mass center	X_I	0
Mass/unit length of the blade	m	7.9529 kg/m
Principal mass moment of inertia of the blade/unit length	I_{MB3}	1.1503×10^{-1} kg.m
	I_{MB2}	6.6723×10^{-3} kg.m

Nonrotating blade frequencies
(Articulated blade)

Flap frequency	$\omega_F = (K_\beta/mR^3)^{\frac{1}{2}}$	0
Lead-lag frequency	$\omega_L = (K_\zeta/mR^3)^{\frac{1}{2}}$	0
Torsional frequency	$\omega_T = (K_\phi/mR^3)^{\frac{1}{2}}$ (Assumed)	1.895 rad/sec
Damping in flap	g_{SF}	0
Damping in lead-lag	g_{SL}	0
Damping in torsion	g_{ST}	0

Vehicle Data

Weight of fuselage F_1	W_{F1}	3.5919×10^4 N
Weight of fuselage F_2	W_{F2}	3.5919×10^4 N
Weight of underslung load	W_{UN}	0.0
Weight of envelope	W_{EN}	8.5539×10^4 N
Weight of supporting structure	W_S	9.4302×10^3 N
Weight of passenger compartment	$W_{S'}$	6.6723×10^3 N

(Treated as a lumped structural load attached at the point O_s on the structure (Fig. 2))

Buoyancy on the envelope	P_z^s	1.3748×10^5 N

Aerodynamic Data

Blade airfoil		NACA 0012
Lift curve slope	a	2π
Lock number	γ	10.9
Solidity ratio	σ	0.0622
Density of air	ρ_A	1.2256 kg/m^3
Blade profile drag coefficient	c_{dO}	0.01
Rotor R.P.M.	Ω	217.79 R.P.M.

Geometric Data

Distance between origin O_s and F_1	ℓ_{F1}	-21.946m
Distance between origin O_s and F_2	ℓ_{F2}	21.946m
Distance between origin O_s and underslung load (Assumed)	h_1	-15.24m
Distance between centerline and rotor hub	h_2	2.591m
Distance between centerline and center of volume of envelope	h_3	14.64m
Distance between centerline and C.G. of the envelope	h_4	8.544m
Distance between origin O_s and C.G. of the structure	h_5	0.0

Structural Dynamic Properties of the Supporting Structure

The supporting structure is modelled as an elastic structure with three normal modes of vibration: two normal modes for bending in vertical and in horizontal plane and one mode for torsion. The two bending modes are symmetric modes and the torsion is an anti-symmetric mode. It was assumed that the envelope and the underslung load are attached to the supporting structure at the origin O_s. The data given above shows that the vehicle is symmetric about Y-Z plane. Furthermore due to the presence of a heavy mass attached at the center (O_s) of the supporting structure, the mode shapes in bending and torsion for each half of the model are assumed to be the modes of a cantilever with a tip mass.

Modal Displacement at F_1, F_2 and O_s

The symmetric mode shape in bending for each half of the supporting structure can be written as [Ref. 11, Page 140]

$$\eta_1 \left(\frac{X}{L}\right) = 6 \left(\frac{X}{L}\right)^2 - 4 \left(\frac{X}{L}\right)^3 + \left(\frac{X}{L}\right)^4$$

(Bending in X-Y plane)

and

$$\eta_2 \left(\frac{X}{L}\right) = 6 \left(\frac{X}{L}\right)^2 - 4 \left(\frac{X}{L}\right)^3 + \left(\frac{X}{L}\right)^4$$

(Bending in X-Z plane)

where X is the coordinate of any section of the supporting structure from origin O_s and L is the length of the supporting structure, L = 21.946m. The mode shape for torsion, for each half of the supporting structure is [Ref. 11, Page 99]

$$\eta_3 \left(\frac{X}{L}\right) = \sin \frac{\pi}{2} \left(\frac{X}{L}\right)$$

Generalized mass and stiffness data

Generalized mass and generalized sitffness for the i^{th} mode of vibration of the supporting structure is defined as

$$M = \int_{F1}^{F2} m\, \eta_i^2\, dx$$

and

$$K = \omega_i^2\, M$$

where ω_i is the i^{th} modal frequency

η_i is the i^{th} mode shape

and m is the mass per unit length (for bending modes, or m is the mass moment of inertia per unit length (for torsion modes).

Bending in x-y plane (horizontal) generalized mass	M_{SBXY}	6.801×10^4 kg
Bending in x-z plane (vertical) generalized mass	M_{SBXZ}	6.801×10^4 kg
Torsion generalized mass	M_{ST}	1.936×10^4 kg.m^2

Appendix B

An equilibrium analysis is carried for the vehicle in hover, using the data given in Appendix A.

Total weight of the vehicle

$$W = W_{EN} + W_S + W_{F1} + W_{F2} + W_{S'} + W_{UN}$$

$$= 8.5539 \times 10^4 + .9430 \times 10^4 + 2 \times 3.5919 \times 10^4$$

$$+ .6672 \times 10^4 + 0$$

$$= 1.7348 \times 10^5 \text{ N}$$

Buoyancy of the envelope $P_z^s = 1.3748 \times 10^5$ N

Weight to be supported by the rotors = 0.36×10^5 N

Thus each rotor has to develop a thrust = 0.18×10^5 N

Since the two rotors are identical and the model vehicle has a symmetry about y-z plane, the equilibrium values for both rotor systems are identical.

They are:

Equilibrium

Flap angle of the blade β_0 = 2.302 degrees

Lead-lag angle ζ_0 = -3.963 degrees

Torsion angle ϕ_0 = -0.115 degrees

Inflow ratio λ = 0.03272

Collective pitch angle of the blade

θ_0 = 4.206 degrees

Thrust coefficient for each rotor

C_T = 0.00158

Buoyancy ratio BR = 0.792

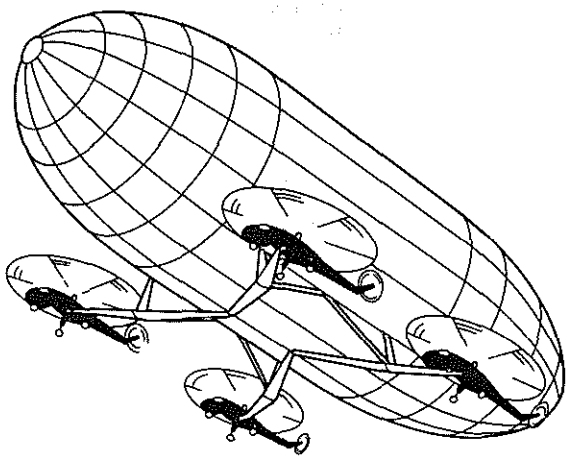

Fig. 1 Hybrid Heavy Lift Helicopter - Approximate Configuration

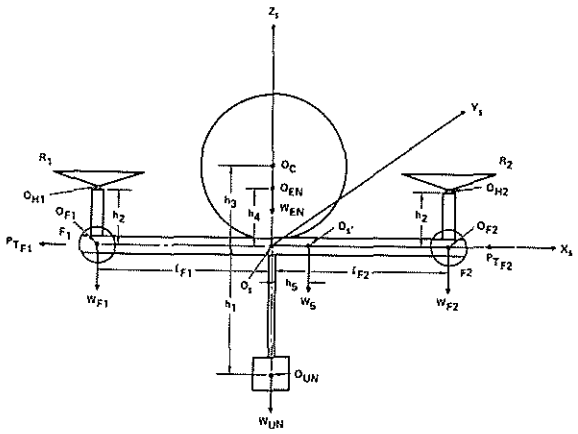

Fig. 2 HHLH Model

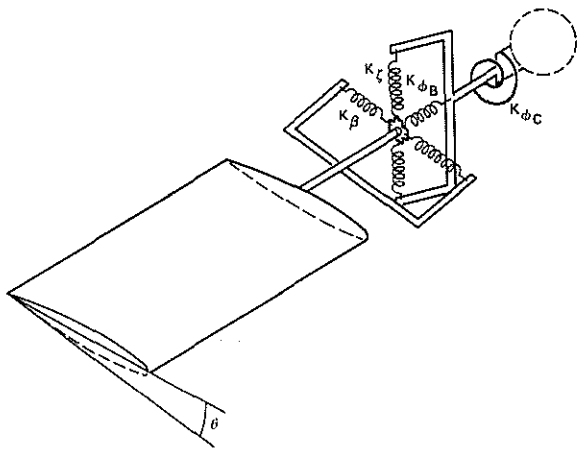

Fig. 3 Equivalent Spring Restrained Blade Model

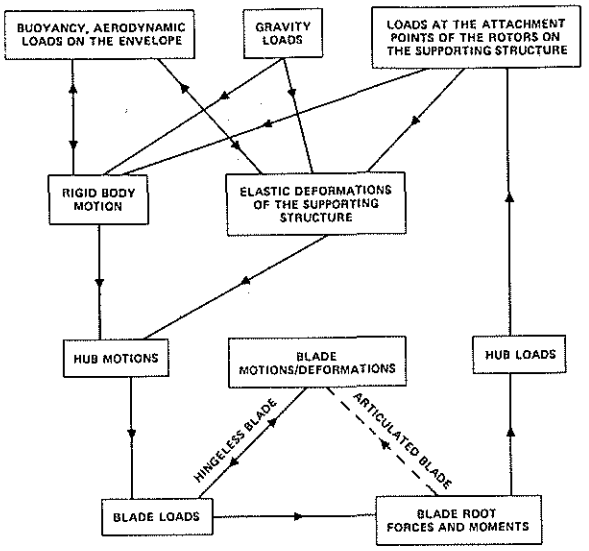

Fig. 4 Schematic Diagram of Coupled Rotor/Vehicle Dynamic Interactions

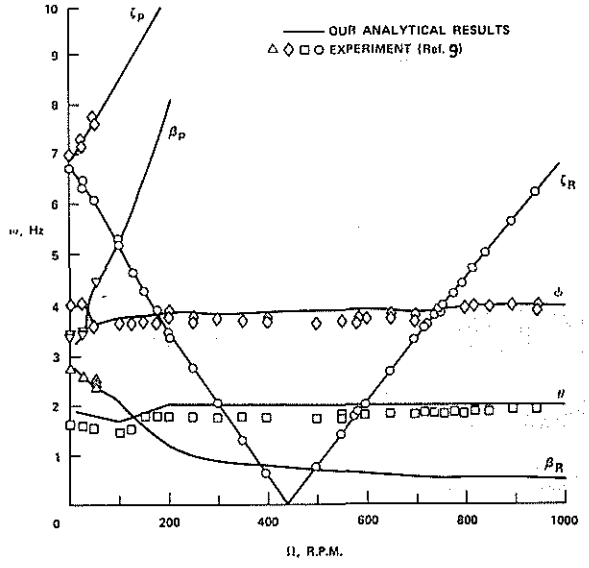

Fig. 5 Modal Frequencies as a Function of Ω, $\theta = 0$

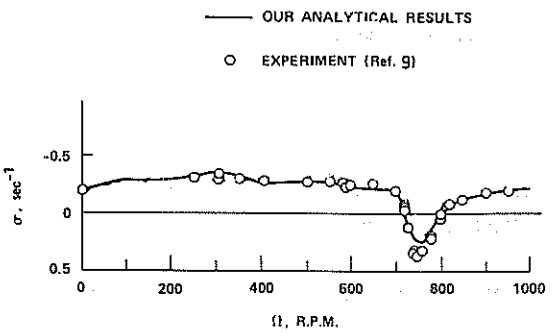

Fig. 6 Regressing Lag Mode Damping as a Function of Ω, $\theta = 0$

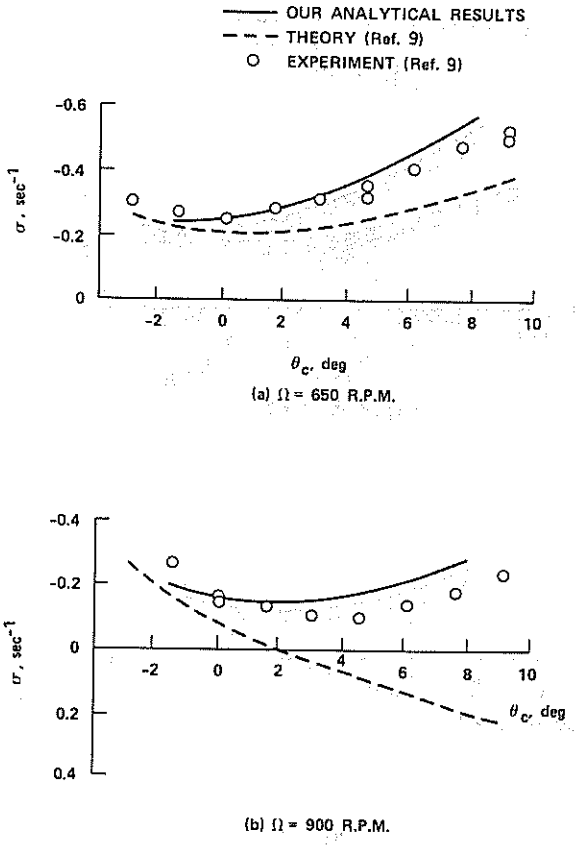

Fig. 7 Lag Regressing Mode Damping as a Function of θ at (a) 650 R.P.M. and (b) 900 R.P.M.

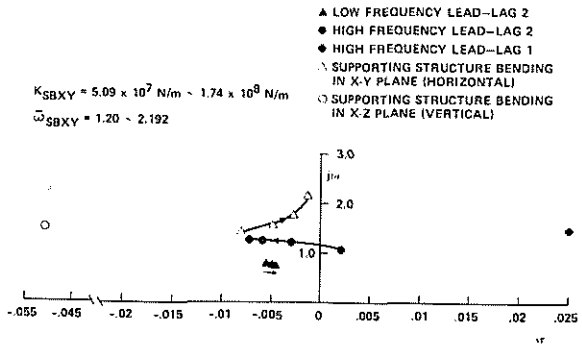

Fig. 8 Variation of Nondimensional Eigenvalues with Increase in K_{SBXY} ($\bar{\omega}_{SBXZ}$ = 1.499, $\bar{\omega}_{ST}$ = 1.096, I_{xx} = 6.44 x 10^5 kg.m^2, I_{yy} = 2.59 x 10^6 kg.m^2, BR = 0.792, C_T = 0.00158)

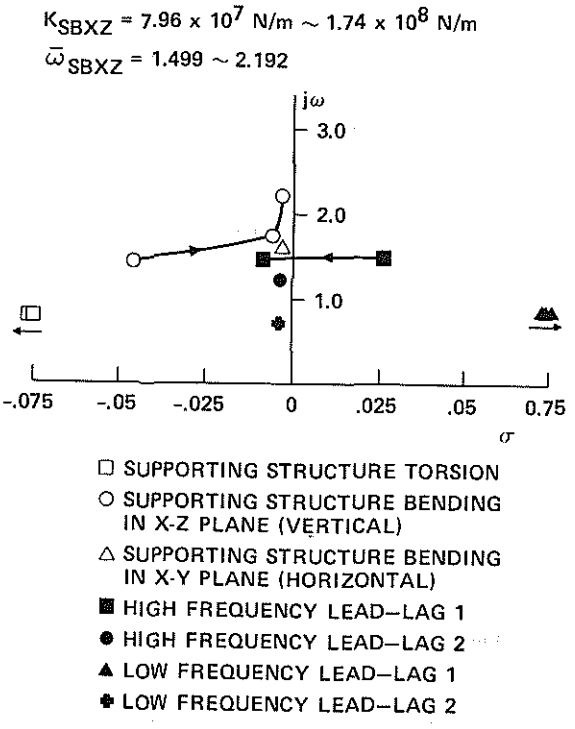

Fig. 9 Variation of Nondimensional Eigenvalues with Increase in K_{SBXZ} ($\bar{\omega}_{SBXY}$ = 1.499, $\bar{\omega}_{ST}$ = 1.096, I_{xx} = 6.44 x 10^5 kg.m^2, I_{yy} = 2.59 x 10^6 kg.m^2, BR = 0.792, C_T = 0.00158)

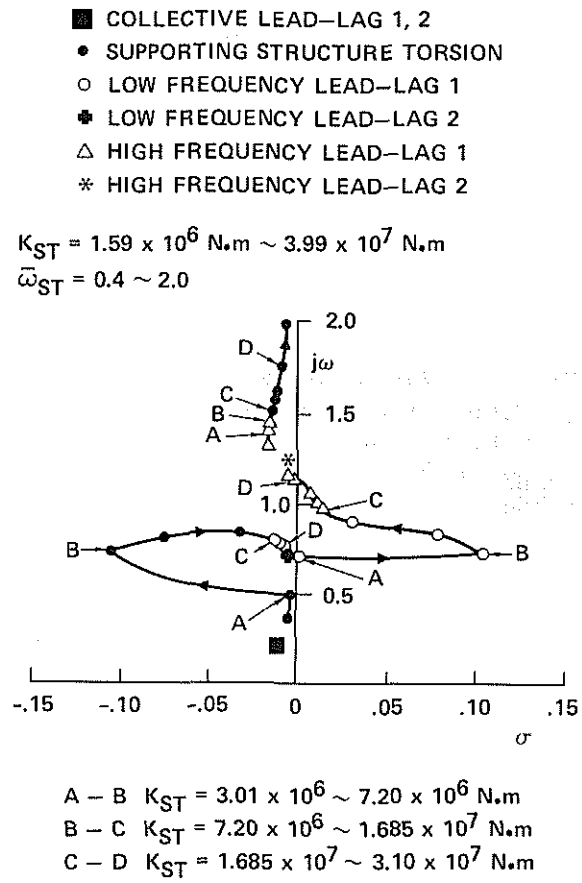

Fig. 10 Variation of Nondimensional Eigenvalues with Increase in K_{ST} ($\bar{\omega}_{SBXY}$ = $\bar{\omega}_{SBXZ}$ = 2.192, I_{xx} = 6.44 x 10^5 kg.m^2, I_{yy} = 2.59 x 10^6 kg.m^2 BR = 0.792, C_T = 0.00158)

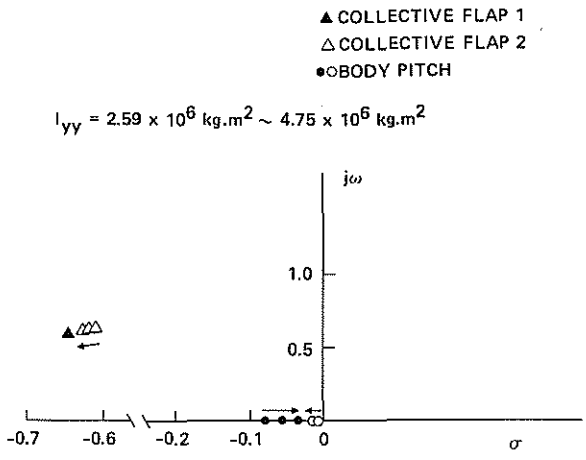

Fig. 11 Variation of Nondimensional Eigenvalues with Increase in I_{yy} ($\bar{\omega}_{SBXY}$ = $\bar{\omega}_{SBXZ}$ = 2.192, $\bar{\omega}_{ST}$ = 1.754, I_{xx} = 2.0 x 10^6 kg.m^2, BR = 0.792, C_T = 0.00158)

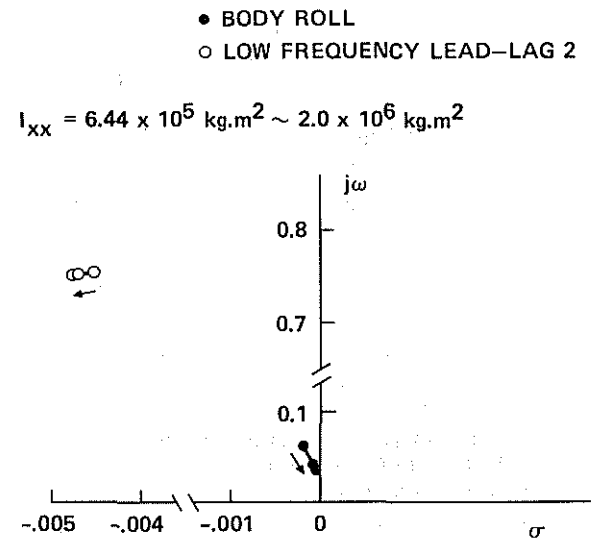

Fig. 12 Variation of Nondimensional Eigenvalues with Increase in I_{xx} ($\bar{\omega}_{SBXY} = \bar{\omega}_{SBXZ} = 2.192$, $\bar{\omega}_{ST} = 1.754$, $I_{yy} = 2.59 \times 10^6$ kg.m^2, BR = 0.792, $C_T = 0.00158$)

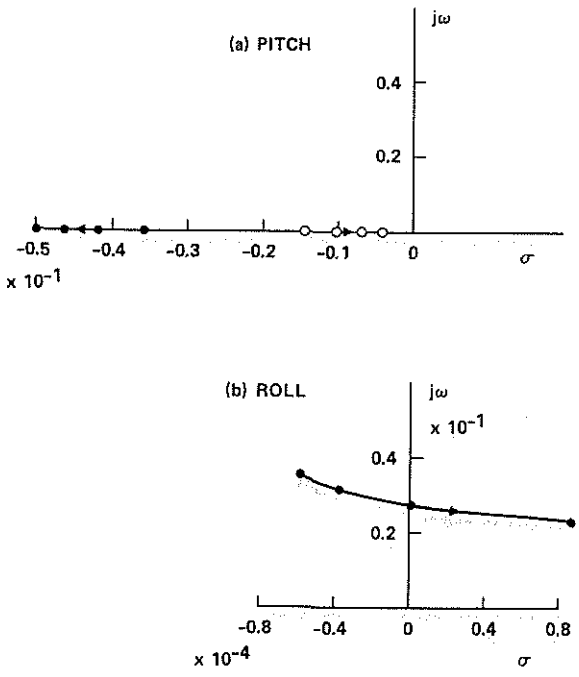

Fig. 14 Variation of Nondimensional Eigenvalues with Decrease in BR, BR = 0.792, 0.7, 0.6, 0.5 ($\bar{\omega}_{SBXY} = \bar{\omega}_{SBXZ} = 2.192$, $\bar{\omega}_{ST} = 1.754$, $I_{yy} = 4.75 \times 10^6$ kg.m^2, $I_{xx} = 2.0 \times 10^6$ kg.m^2)

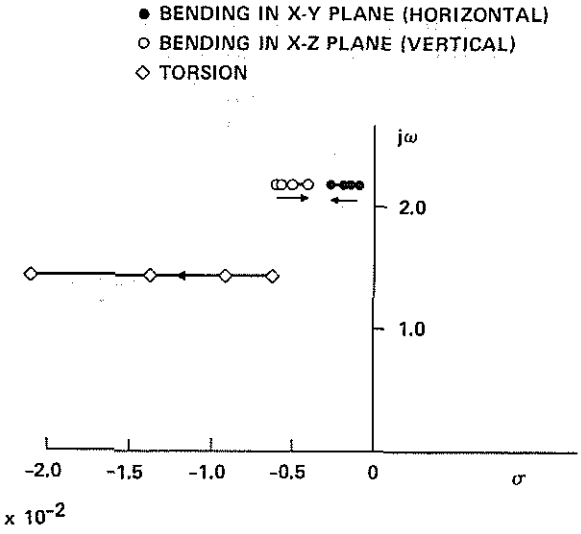

Fig. 13 Variation of Nondimensional Eigenvalues with Decrease in BR, BR = 0.792, 0.7, 0.6, 0.5 ($\bar{\omega}_{SBXY} = \bar{\omega}_{SBXZ} = 2.192$, $\bar{\omega}_{ST} = 1.754$, $I_{yy} = 4.75 \times 10^6$ kg.m^2, $I_{xx} = 2.0 \times 10^6$ kg.m^2)